Chemical and Process Engineering Research
ISSN 2224-7467 (Paper) ISSN 2225-0913 (Online)
Vol.23, 2014

A simple Simulation Model for Oxidative Coupling of Methane over $La_{0.6}Sr_{0.4}NiO_3$ Nanocatalyst.

Delvin Aman[1*] Tamer Zaki[1] Sara Mikhail [1] Mohamed Ali[2]

1. Egyptian petroleum Research Institute, PO box 11727, Cairo, Egypt

2. Department of Chemical Engineering, Faculty of Engineering, Cairo University, Cairo, Egypt

* E-mail of the corresponding author: delvinaman@yahoo.com

Abstract

$La_{0.6}Sr_{0.4}NiO_3$ perovskite-type oxides were prepared by reverse microemulsion method aided by ultrasonic homogenizer. The mixed oxide precursors and the corresponding derived fresh catalysts were characterized by thermogravimetry and differential thermal analysis (TG/DTA), X-ray diffraction (XRD), Brunauer–Emmett–Teller (BET) surface area and high resolution transmission electron microscope (HRTEM). XRD results reveal that pure phase of perovskite-type crystalline structure was obtained for all samples and the electronic unbalance caused by the partial substitution for La^{3+} by Sr^{2+} is compensated by oxidation of a fraction of Ni^{3+} to Ni^{4+} and/or generation of oxygen vacancies in the perovskite lattice. There exist two kinds of oxygen species on the oxides: surface adsorption oxygen and bulk lattice oxygen. The surface oxygen contributed to oxidize methane completely to CO_2 and H_2O because of its higher reactivity, while the other one prone to oxidative coupling of methane into C_2H_6 and C_2H_2 (C_{2+}). In this study a mathematical model for the oxidative coupling of methane (OCM) over $La_{0.6}Sr_{0.4}NiO_3$ pervoskite is developed. From this simulation it can predict that the activity at temperature ≥ 925 ºC and methane partial pressure =0.3 and oxygen partial pressure =0.1 will be reach ~10% and selectivity ~50%.

Keywords: Oxidative coupling, Methane, Perovskite

1. Introduction

In the past two decades, considerable world-wide researches have been conducted to develop various commercially viable processes for methane conversion via direct or indirect routes. Among these researches, the direct route that converts methane into high hydrocarbons in one step by the oxidative coupling reactions is more economically attractive and consequentially has been thoroughly studied (Siavash et al. 2011). Investigations made on OCM have been mostly focused on the two following areas: a) Synthesis and characterization of catalysts, determination of active sites and the role of promoters, and

b) Kinetic studies, investigation of mechanisms and measurement of activation energies.

So far a large number of catalysts and kinetics of this reaction have been reported in the literature (Nastaran et al. 2010), it is necessary to find a catalyst that could activate the C–H bond of cyclohexane and provide moderately active oxygen atoms so as to avoid the nonselective oxidation to CO and CO_2 (Jin et al. 2009). Perovskite-type oxides, represented by the general formula ABO_3, were found very active and selective toward C_{2+} hydrocarbons.

In particular, the role of the A site ion is to stabilize the perovskite structure, while the B-site ion is relevant to the catalytic activity. The high stability of the perovskite structure allows the partial substitution of either A or B cations by other metals with different oxidation states, can change the electronic state, oxidation state, M–O bond strength, and generate a higher average oxidation state of the B ion or the formation of oxygen vacancies. The oxygen vacancies play an important favorable role in the oxidation process since they accelerate the dissociation of oxygen molecules on the surface and increase the mobility of lattice oxygen. These situations are usually reached by partial replacement of the A cation (La) with other metals (as Sr), which can have an oxidation state different from 3+ (Barbero et al. 2006). Kinetic studies, reaction modeling and simulation can be used for the interpretation and optimization of the data that obtained from the homogeneous and heterogeneous reactions. It can predict the effects of different operating conditions which reduced the required experimental work (Lee et al. 2012). The simulations were done by using the polymath software program to estimate the rates of methane conversion, C_{2+} and CO_x formation; the methane conversion and selectivity to C_{2+}.

2. Experimental

2.1. Catalyst preparation

In the single-reverse microemulsion technique, just one reverse microemulsion is used. The reverse microemulsion used for this study consisted of CTAB as surfactant (s), 1-butanol as co-surfactant (cs), and cyclohexane as oil phase (o). In all of the reverse microemulsions, the mass ratio of (cs) to (s) was 1.5. An aqueous solution (w) of $LaCl_3 \cdot 7H_2O$ (Sigma, assay 99.9%), $Sr(NO_3)_2$ (Eastrin Fine Chemicals, Ltd, assay 95%) and $Ni(NO_3)_2 \cdot 6H_2O$ (Eastrin Fine Chemicals, Ltd, assay 99%) containing a total metal concentration of 1M was added drop wise to four different ratios of the mixture (s + cs):(o) for mass ratios of 0.2 (A1), 0.4 (A2), 0.6 (A3), and 0.8 (A4). In Figure 1, the compositions of the microemulsions used for this study are shown with the aid of a triangle diagram. In this diagram, the initial (s + cs) :(o) ratios (0.2, 0.4, 0.6 and 0.8) are shown on the base of the triangle. The addition of $LaCl_3 \cdot 7H_2O$, $Sr(NO_3)_2$ and $Ni(NO_3)_2 \cdot 6H_2O$ took place upwards along the dashed lines A1–A4. During the addition of the aqueous mixture of salts, $LaCl_3 \cdot 7H_2O + Sr(NO_3)_2 + Ni(NO_3)_2 \cdot 6H_2O$, into the (o) + (s) + (cs) mixtures, the conductivity (σ) of the solution was affected. The variation in conductivity was studied using a bench top Hanna conductivity meter kept at 25 °C with circulating water from a controlled temperature stabilizer. The obtained results are shown in Figure 2 in the form $\sigma = f(\varphi)$. The fraction φ is equal to $V_w/(V_w + V_o + V_s + V_{cs})$, where V_w is the volume of aqueous phase, V_o is the volume of oily phase, V_s is the volume of surfactant, and V_{cs} is the volume of co-surfactant. The volume of surfactant (V_s) was not taken into account since the volume of CTAB as a solid was negligibly small. In the triangular diagram shown in Fig. 1, we have chosen one point (A) corresponding to microemulsion A4 for preparing perovskite $La_{0.6}Sr_{0.4}NiO_3$. The corresponding perovskite was developed by adding an aqueous NH_4OH solution (4M) to the vigorously stirred microemulsion A4 as a precipitating agent. The hydroxide mixture was then filtered, washed alternatively three times with deionized water and an alcohol mixture, and then dried at 100 °C overnight. The dried powder was ground in an agate mortar and calcined at 750 °C for 4 h under atmospheric conditions. The final calcination temperature 800 °C was selected after thermogravimetric investigation.

2.2. Catalyst characterization

2.2.1. Thermal measurements (DTA-TGA)

Differential thermal analysis was carried out by Q600 DST simultaneous DSC/TGA apparatus. All runs were carried out at a heating rate of 10ºC/min in the temperature range from room temperature to 1000ºC under nitrogen flow to follow the structural changes accompanying the thermal treatment.

2.2.2. XRD measurements

The crystalline structure of the prepared powder was analyzed by X-ray diffractometry (XRD) (X-Pert PRO, PAN analytical, Netherlands) using CuK_ radiation in the angular region of 2θ=4°–70°. For phase identification purposes, automatic JCPDS library search and match were used.

2.2.3. BET surface area measurements

Brunauer-Emmett-Teller (BET) surface area was measured at liquid nitrogen temperature (-196ºC) using Quantachrome Nova 3200 S automates gas sorption apparatus. Prior to such measurements all samples were perfectly degassed at 300ºC for six hours and under vacuum pressure 1.3 x 10^{-3} Pa.

2.2.4. Transmission electron microscope (TEM) measurements

Transmission electron microscopy images were recorded on a JEOL-1400 TEM at 120 kV.

2.3. Kinetic modeling and reaction rates

A gas-phase heterogeneous kinetics is studied to assess the capability of the prepared perovskite $La_{0.6}Sr_{0.4}NiO_3$ catalyst towards the oxidative coupling of methane that be carried out in fixed-bed reactor at different conversion conditions.

The C_{2+} production, carbon oxides (CO_x) formation, and methane conversion rates are explained as functions of methane and oxygen partial pressure under experimental conditions of: weight of catalyst 0.05g , $0.15 \geq P_{CH4} \leq 0.3$ atm, P_{O2} =0.1atm, and at reaction temperature range 800º C ≥ T≤ 925º C (Taheri et al. 2009).

The reaction scheme for the OCM is considered as follows:

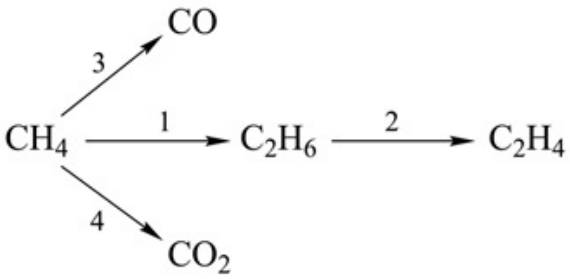

The detailed elementary steps are:

$$2CH_4 + 0.5O_2 \longrightarrow C_2H_6 + H_2O$$

$$C_2H_6 + 0.5O_2 \longrightarrow C_2H_4 + H_2O$$

$$CH_4 + 1.5O_2 \longrightarrow CO + 2H_2O$$

$$CH_4 + 2O_2 \longrightarrow CO_2 + 2H_2O$$

The power law model is selected by (Farsi et al. 2011) to estimate the reaction rate in terms of partial pressures of methane and oxygen:

$$R_i = K P_{CH_4}^m P_{O_2}^n \qquad (1)$$

where, the rate constants were calculated by the Arrhenius equation:

$$K = k_0 \exp\left(\frac{-E}{RT}\right) \qquad (2)$$

in which k_0 is the pre-exponential factor and E is the activation energy.

The parameters in the power law model are solved by applying the polymath program.

The following equations (3−5) represent the results that obtained from the kinetic power law model, including the pre-exponential factor (k_0), activation energy (E_i) and power law exponents (m, n):

$$R_{CH_4} = 5.375443 e^{\frac{-1049527}{RT}} P_{CH_4}^{0.39563} P_{O_2}^{0.72761} \qquad (3)$$

$$R_{C_{2+}} = 0.108777366 e^{\frac{-833277.7}{RT}} P_{CH_4}^{0.6541} P_{O_2}^{0.618} \qquad (4)$$

$$R_{CO_x} = 5.375443 e^{\frac{-1049527}{RT}} P_{CH_4}^{0.39563} P_{O_2}^{0.72761} - 0.217554732 e^{\frac{-833277.7}{RT}} P_{CH_4}^{0.6541} P_{O_2}^{0.618} \qquad (5)$$

These kinetic equations are basically taken from the experimental data published by (Farsi et al. 2011) who used a nano structured perovskite catalyst that is similar to the selective perovskite $La_{0.6}Sr_{0.4}NiO_3$ catalyst towards the oxidative reaction under the same experimental condition in our pervious work (Aman et al. 2013).

3. Results and discussion

Fig. 2 shows that a gradual increase in φ (aqueous ratio) results in an increase in conductivity (σ), because both the number and the size of the micelles increase. The conductivity maximum can be attributed to the saturation of the micelles and the percolation phenomenon (Koˇsak et al. 2004). When more water was added to the system, it led to a phase separation, and conductivity was lowered. The point (P) in Fig. 2 is the saturation point. The larger the region between the initial and maximum conductivity, the greater the W/O micelle region, and the

better the system is for producing a microemulsion (Li et al. 2003).

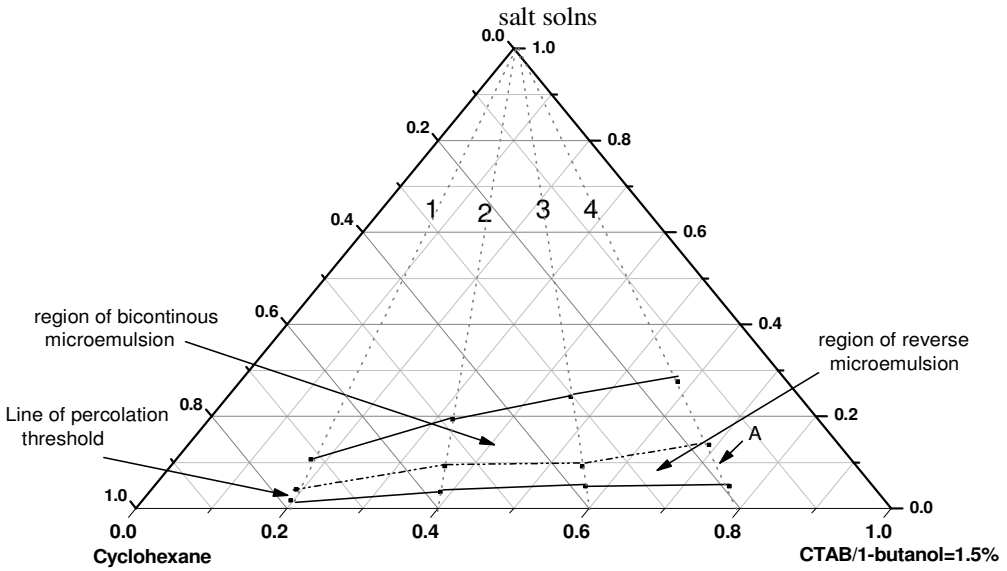

Figure 1. Phase diagram of the reverse microemulsion system for $La_{0.6}Sr_{0.4}NiO_3$ at TMC =1. The conductivity experiments in figure 2 were performed along the dotted lines (…..). The upper bold line (–) corresponds to the upper limits of the experiment. The dashed dotted line (.-.-) corresponds to the maximum of dσ/dφ curves in Figure 3 and roughly divides the region of the reverse from that of bicontinuous microemulsion. The lower bold line is the approximate limit at the percolation threshold. The point X_1 corresponds to the composition chosen for the synthesis of perovskite.

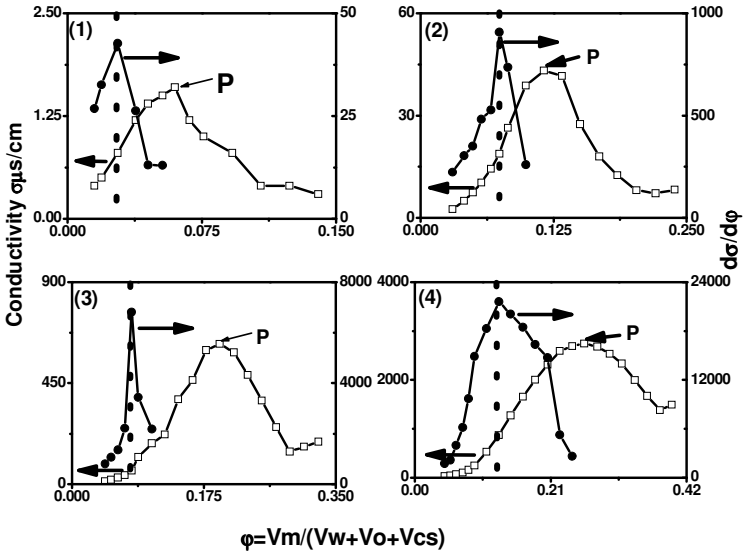

Figure 2. Variation of the conductivity σ of the system to prepare $La_{0.6}Sr_{0.4}NiO_3$ at TMC =1 by the addition of the aqueous solution (▫).The variation of dσ/dφ= f (φ) is also shown. The dashed vertical line separates roughly the reverse region (left) and bicontinuous region (right) of microemulsion (●).

3.1. Physicochemical properties of catalyst

The reaction process during the thermal treatment can be described as follow:

$$0.6LaCl_3 + Ni(NO_3)_2 + 0.4Sr(NO_3)_2 + 3.6NH_4OH \longrightarrow$$

$$0.6La(OH)_3 + 0.4Sr(OH)_2 + Ni(OH)_2 + 1.8NH_4NO_3 + 1.8NH_4Cl \quad (1)$$

$$0.6La(OH)_3 + Ni(OH)_2 + 0.4Sr(OH)_2 \xrightarrow{\triangle}$$

$$0.3La_2O_3 + NiO + 0.4SrO + 2.3H_2O \quad (2)$$

$$0.3La_2O_3 + NiO + 0.4SrO + 0.7O_2 \xrightarrow{\triangle} La_{0.6}Sr_{0.4}NiO_3 \quad (3)$$

For the prepared $La_{0.6}Sr_{0.4}NiO_3$ sample, differential thermal profile Figure 3 exhibits a large endothermic peak centered at 227 °C accompanied by a loss in weight due to the escape of adsorbed water and also to the decomposition of the surfactant. The three endothermic peaks that appear at ~ 327, 340 and 495°C are related to the decomposition of $Ni(OH)_2$, $La(OH)_3$ and $Sr(OH)_2$, respectively into their oxides (Oliveira et al. 2010). Also these endothermic effects are accompanied by a high loss in weight (~17 wt %).The weight loss was about 17 wt %which is in agreement with the theoretical value of 16.2 wt% caused by the loss of 2.3 molecules of water (Eq. (2)). Another small endothermic peak appears at 678°C assigned to the formation of $La_{0.6}Sr_{0.4}NiO_3$ perovskite sample according to the sequence of steps of the reaction during the thermal treatment (Eq. (3)).

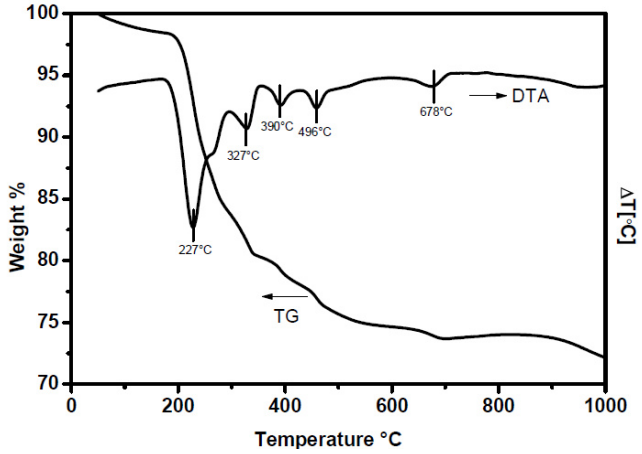

Figure 3. Differential and gravimetric thermal profiles of perovskite $La_{0.6}Sr_{0.4}NiO_3$ sample.

The XRD patterns (figure 4) of the $LaNiO_3$ and $La_{0.6}Sr_{0.4}NiO_3$ samples. Both samples exhibited single crystalline perovskite structure. The diffraction lines of $LaNiO_3$ could be indexed to standard $LaNiO_3$ (JCPDS file No. 33-0711) with a rhombohedral structure, while the Sr-substituted sample ($La_{0.6}Sr_{0.4}NiO_3$) exhibited an almost identical diffraction pattern to cubic $LaNiO_3$ (JCPDS file No. 33-0710). This mean the strontium substitution could induce changes in the crystalline structure there by modifying the rhombohedral structure tending to a nearly cubic one. This means that the substituted perovskite structures are less distorted than that of $LaNiO_3$ (Kumar et al. 2013).

Accordingly, the high ionic radius of 12-coordinated Sr^{2+} (1.44 Å) as compared to that of 12-coordinated La^{3+} (1.36 Å) indicates that the cell volume should be very slightly affected by the strontium substitution. Nevertheless, as the strontium has a lower oxidation state than lanthanum, an increase of the nickel oxidation state from Ni^{3+} to Ni^{4+} could have occurred or oxygen vacancies would be generated to maintain the structure electroneutrality. The ionic radius of Ni^{4+} (0.48 Å) is smaller than that of Ni^{3+} (0.56 Å); then, this could be the reason for the slight increase in cell volume.

Figure 4. X-ray differaction patterns of perovskite $LaNiO_3$ and $La_{0.6}Sr_{0.4}NiO_3$ samples.

The data in table (1) indicates that the electronic debalance for the prepared $La_{1-x}Sr_xNiO_3$ sample has been affected by the partial substitution of lanthanum (3+) with strontium (2+). The tolerance factor (t) was defined

using Goldschmid's equation:

$$t = \frac{r_A + r_O}{\sqrt{2}(r_B + r_O)}$$

where r_A, r_B and r_O represent the ionic radii of A and B cations, and the O anion for ABO_3-type compounds (Barbero et al. 2006).

The perovskite structure exists in oxides within the t range 0.75-<1. The value 1 is for cubic perovskite and it decreases when the structure is distorted. Then, the increase in the value t with the increase in the strontium substitution level indicates a tendency of the structure towards a nearly cubic one, which was confirmed from the XRD results.

Table (1): Structural parameters of $LaNiO_3$ and $La_{0.6}Sr_{0.4}NiO_3$

Sample	**Crystalline phase**	**a* (Å)**	**V**(Å^3)**	**t*** **
$LaNiO_3$	Rhombohedral	3.861	57.55	0.83
$La_{0.6}Sr_{0.4}NiO_3$	Cubic	3.876	58.21	0.84

The adsorption isotherms of all samples are Type II according to Brunauer classification. As shown in Figure 5, there is no hysteresis loop thus $La_{0.6}Sr_{0.4}NiO_3$ has no internal porosity owing to the lack of a pronounced hysteresis loop in each. Therefore the calculated specific surface areas (S_{BET} = 20.8 m^2/g) are mainly related to the external surface formed between the small particles (Giannakas et al. 2004).

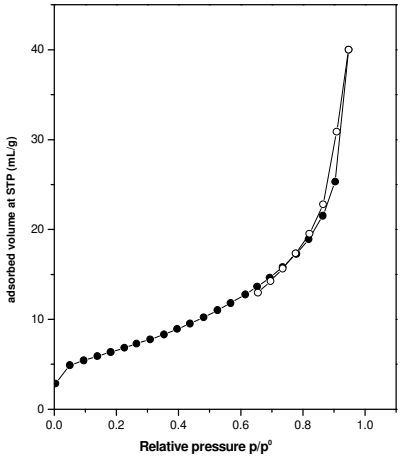

Figure 5. Adsorption-desorption isotherms for perovskite $La_{0.6}Sr_{0.4}NiO_3$ sample.

TEM image Figure 38 show that the shape of the particles is mostly square and their particle sizes are almost uniform. The discrepancy in the crystallite diameter data (14.1 nm) confirmed by the x-ray diffraction analysis with that by TEM (10.8–33.1) is due to the agglomeration among the primary particles (Biswas 2009)**.** One the other hand this solid is non-rigid aggregates of plate-like particles (in agreement with N_2 adsorption-desorption data).

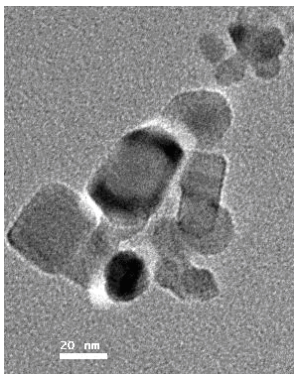

Figure 6. TEM image of $La_{0.6}Sr_{0.4}NiO_3$ perovskite sample.

3.2. Kinetic modeling and reaction rates

The conversions of methane are calculated according to the following equation [16]:

$$X_{CH4} = R_{CH4}. W/ F_{input,CH4} \quad (6)$$

where X_{CH4}, R_{CH4}, W and $F_{input,CH4}$, are the methane conversion value , overall conversion rate of methane, catalyst mass and methane input molar flow rate, respectively.

Figure 7 shows the calculated methane conversion rates as a function of methane partial pressures at the reaction temperature range 800-925° C. Data in figure clarifies that the rate of methane exhibits high values at higher reaction temperatures. On the other hand the rate of methane conversion increases continuously by increasing the partial pressure of methane. Therefore, high temperature conditions are necessary to activate the strong primary C–H bonds in the reactants; more methane is consumed and the conversion increases.

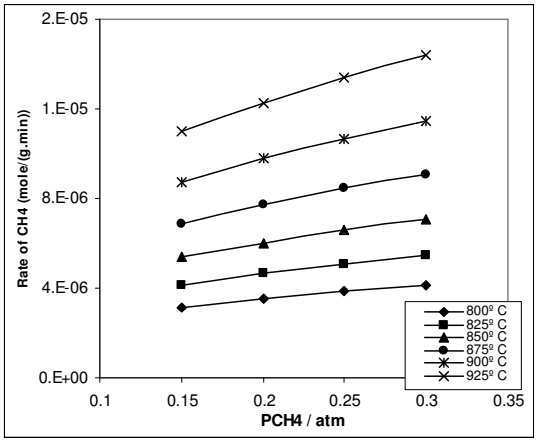

Figure.7. Calculated methane conversion rates at different reaction temperatures as a function of methane partial pressure.

Figures 8 and 9 show the calculated rates of C_{2+} and CO_x formation as a function of methane partial pressure at different reaction temperatures. As expected, more C_{2+} is formed at higher temperatures because more CH_4 is consumed as previously represented in Figure. 7.

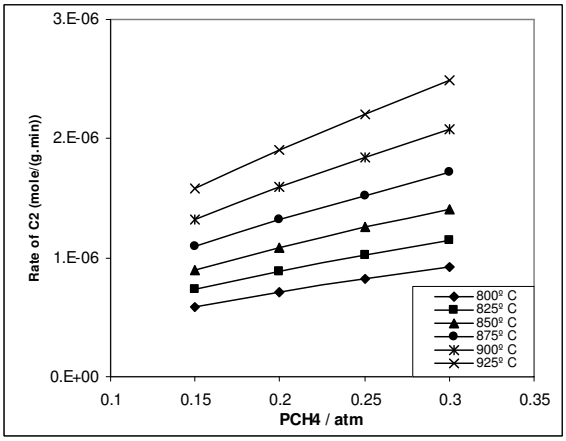

Figure .8. Calculated C_{2+} formation rates at different reaction temperatures as a function of methane partial pressure.

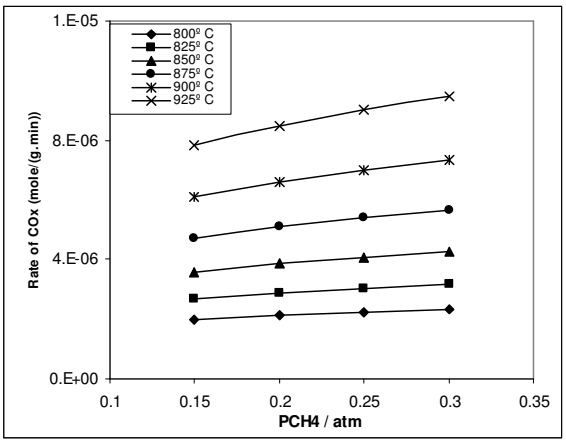

Figure .9. Calculated CO_x formation rates at different reaction temperatures as a function of methane partial pressure.

From the relation between the CH_4 conversion and the reaction temperatures at different partial pressure of methane Figure10, it's clear that the conversion of methane increases with the reaction temperature as well as the increase in methane partial pressure. On the other hand, the selectivity of the prepared nano $La_{0.6}Sr_{0.4}NiO_3$ perovskite catalyst towards the converted C_{2+} increases by increasing the reaction temperature and follows almost the same trend, regardless of different methane partial pressure (histogram-Figure. 11).

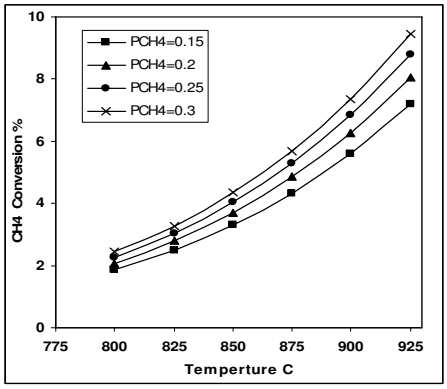

Figure 10. Calculated methane conversion at different reaction temperatures for different methane partial pressures.

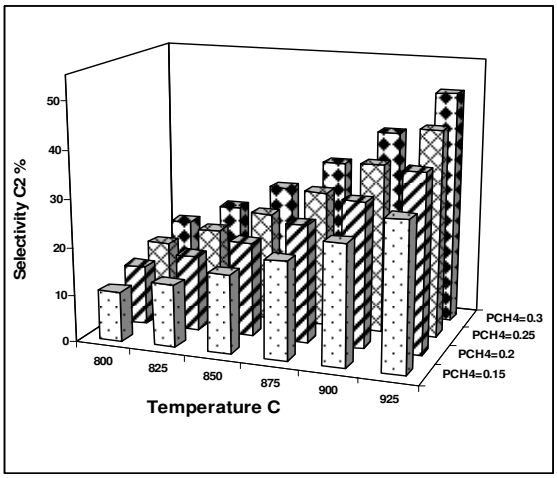

Figure11. Calculated C_{2+} selectivity at different reaction temperatures for different methane partial pressures.
From figure 11, this simulation can predict that activity at temperature ≥ 925 ºC and methane partial pressure =0.3 and oxygen partial pressure =0.1 will be reach ~10% and selectivity ~50%.

4. Conclusion

Kinetic simulation of OCM reaction was developed over $La_{0.6}Sr_{0.4}NiO_3$ nanocatalyst which was synthesized by reverse microemulsion method. It is suggested that a simple power law kinetic model may assist the researchers in computer aided program (polymath). It can be useful for estimating the methane conversion and C2+ selectivity under the considered conditions. In order to propose a simple kinetic model over this nanocatalyst, many available mechanisms were surveyed and four reaction steps were chosen which, are the most important reactions leading to OCM products and common among all the available mechanisms. The accuracy of the kinetic model was evaluated by comparing with the experimental data. The results showed that the power law model can be used for kinetic modeling of OCM with its own limitations. This simulation can predict that activity at temperature ≥ 925 ºC and methane partial pressure =0.3 and oxygen partial pressure =0.1 will be reach ~10% and selectivity ~50%.

References

Nastaran, R. F., Ali, V., Shahrnaz., (2010), "Kinetic simulation of oxidative coupling of methane over perovskite catalyst by genetic algorithm: Mechanistic aspects" J. Nat. Gas. Chem, **19**, Elsevier, 385-392. DOI: 10.1016/S1003-9953(10)60206-X

Jin, M., Cheng, Z., Gao, Y., Fang, X., (2009), "Oxidative dehydrogenation of cyclohexane with $Mg_3(VO_4)_2$synthesized by the citrate process" Mat. Lett., **63**, Elsevier, 2055- 2058. DOI: 10.1016/j.matlet.2009.06.054

Barbero, B. P., Gamboa, J.A., Cadús, L. E., (2006) "Synthesis and characterisation of $La_{1-x}Ca_xFeO_3$ perovskite-type oxide catalysts for total oxidation of volatile organic compounds" Appl. Catal. B, **65**, Elsevier, 21-30. DOI: 10.1016/j.apcatb.2005.11.018

Lee, M.R., Park, M-J, Jeon, W., Choi, J-W., Suh, Y-W., Suh, D.J., (2012) "A kinetic model for the oxidative coupling of methane over Na2WO4/Mn/SiO2" Fuel Processing Technology **96**, Elsevier,175–182. DOI: 10.1016/j.fuproc.2011.12.038

Taheri, Z., Seyed-Matin, N., Safekordi, A.A., Nazari, K., Pashne, S. Z., (2009) "A comparative kinetic study on the oxidative coupling of methane over LSCF perovskite-type catalyst" Appl. Catal. A, **354**, Elsevier,143-152. DOI: 10.1016/j.apcata.2008.11.017

Farsi A., Ghader S., Moradi, A., Mansouri, S.S., Shadravan, V., (2011) "A simple kinetic model for oxidative coupling of methane over $La_{0.6}Sr_{0.4}Co_{0.8}Fe_{0.2}O_{3-\delta}$ nanocatalyst" J. Nat. Gas. Chem., **20**, Elsevier,325-333. DOI: 10.1016/S1003-9953(10)60179-X

Aman D. (2013), "Preparation of Perovskite Catalyst for Oxidative Reactions" Ph.D. thesis, physical chemistry department, Ain shams university.

Košak, A., Makovec, D., Drofenik, M.,

(2004) "The preparation of MnZn-ferrite nanoparticles in a water/CTAB, 1-butanol/1-hexanol reverse microemulsion", Phys. Stat. Sol. C, **1**, WILEY-VCH Verlag GmbH & Co. KGaA, Weinheim,3521–3524. Doi: 10.1002/pssc.200405495

Li F.; Vipulanandan C.; Mohanty K.K.; (2003) "Microemulsion and solution approaches to nanoparticle iron production for degradation of trichloroethylene" Coll. Sur. A., **223** , Elsevier,103-112. DOI: 10.1016/S0927-7757(03)00187-0

Oliveira F.S.; Pimentel P.M.; Oliveira R.M.P.B.; Melo D.M.A.; Melo M.A.F.; (2010) "Effect of lanthanum replacement by strontium in lanthanum nickelate crystals synthetized using gelatin as organic precursor" Mat. Lett. **64**, Elsevier, 2700-2703. DOI: 10.1016/j.matlet.2010.08.059

Kumar D. A.; Selvasekarapandian S.; Nithya H.; Leiro J.; Masuda Y.; Kim S-D.; Woo S-K.; (2013) "Effect of calcium doping on $LaCoO_3$ prepared by Pechini method" , Powder Technol. **235** , Elsevier, 140-147. DOI: 10.1016/j.powtec.2012.09.030

Giannakas A.E., Ladavos A.K, Pomonis. P.J., (2004), "Preparation, characterization and investigation of catalytic activity for NO+CO reaction of $LaMnO_3$ and $LaFeO_3$ perovskites prepared via microemulsion method "Appl Catal B, **49**, Elsevier,147-158. DOI: 10.1016/j.apcatb.2003.12.002

Biswas M. (2009), "Synthesis of single phase rhombohedral $LaNiO_3$ at low temperature and its characterization" J. Alloys Compd., **480**, Elsevier, 942-946. DOI: 10.1016/j.jallcom.2009.02.099